14th International Symposium on Turbulence and Shear Flow Phenomena (TSFP14)
Heidelberg, Germany, July 28–31, 2026

MEASUREMENTS OF THE UNSTEADY WALL SHEAR STRESS VECTOR IN THE TURBULENT PIPE FLOW UP TO RE$_\tau$ = 28 000

Joachim Klinner, Christian Willert
DLR Institute of Propulsion Technology
German Aerospace Center
51170 Köln, Germany
chris.willert@dlr.de · joachim.klinner@dlr.de

Lorenzo Magnani, Alessandro Talamelli, Gabriele Bellani
Department of Industrial Engineering / CIRI Aerospace
University of Bologna
Forlì, Italy
lorenzo.magnani9@unibo.it · alessandro.talamelli@unibo.it · gabriele.bellani2@unibo.it

ABSTRACT

Three-dimensional particle tracking velocimetry (PTV) was conducted in the turbulent boundary layer of the CICLoPE long pipe test facility using a single-camera multi-aperture 3d 3c micro PTV system. The wall distance of imaged particle is encoded in the size of particle imaged triplets that are formed by a triple aperture placed in the optical path, following the "defocusing" concept originally described by Willert & Gharib (1992). In contrast to previously published multi-aperture microscopic particle tracking velocimetry (MA-µPTV) in a canonical turbulent boundary layer (TBL) using a back-scattering configuration (Klinner & Willert, 2025), the present setup illuminates the particles from the side which achieves a higher scattering efficiency and mitigates light scatter at the air-glass interface. Thereby, the number density of successfully reconstructed particle triplets is roughly doubled which improves spatial resolution and statistical convergence. Extensive image data of the turbulent pipe BL was recorded for center line velocities of $5.2 \leq U_{\mathrm{cl}} \leq 30.1$ m/s with corresponding shear Reynolds numbers of $5700 \leq \mathrm{Re}_\tau \leq 28\,100$. The recovered PTV data sets provide velocity statistics up to the fourth moment up to wall distances of 600 µm and capture the near-wall turbulence peak. In addition, both the stream- and spanwise fluctuations of the wall shear stress (WSS) vector and accelerations within the viscous sub-layer are estimated. Probability distributions of the WSS vector exhibit no particular Reynolds number trend.

INTRODUCTION

The CICLoPE facility (Centre for International Cooperation in Long Pipe Experiments), operated by the University of Bologna, is a unique research center for investigating turbulence in aeronautical flows. It enables the generation of flows with high Reynolds numbers of up to $Re_{\tau,\max} \approx 50\,000$, while still allowing the measurement of viscosity scales in the range of 10 µm. The facility has a 100-meter long pipe with a diameter of 900 mm, in which stable dynamic and thermal conditions can be maintained (Talamelli *et al.*, 2009).

The present contribution represents an attempt to extend the MA-µPTV technique recently validated for unsteady WSS measurements in a canonical planar TBL (Klinner & Willert, 2025) to pipe boundary layers. The measurements build on experience gained from earlier high-speed profile PIV measurements carried out by the authors at the CICLoPE (Willert *et al.*, 2017), whereby the previous tunnel insert was modified to include an additional access port to facilitate 3d tracking of particles illuminated from the side by a thick laser sheet.

EXPERIMENTAL METHOD

As outlined in Fig. 1(a), the high-speed camera (Vision Research T4040) and an infinity-corrected microscope lens (Mitotuyo Plan Apo 5×) image particles through a cylindrical window that matches the inner contour of the pipe ($R = 450$ mm). The objective is combined with a tube lens of $f = 180$ mm. In that way a field of view (FOV) of 3.7 mm × 1.4 mm can be captured at an image size of 2048 × 768 pixel at a frame rate of 20 kHz.

The pinhole mask consists of a black anodized aluminum foil and is placed in the nearly parallel optical path between the objective and the tube lens. The mask contains three precision-milled pinholes, each with 2 mm diameter, that form an equilateral triangle. The spacing between the pinholes is maximized such that the apertures are located within the entrance pupil diameter of the objective. The size of the triplet image of a particle projected through this triplet aperture varies linearly with the radial position of particles along y. The depth sensitivity of the microscopic setup is 89.3 pixel/mm which corresponds to an uncertainty in radial position of 5 µm when assuming an uncertainty of 0.5 pixel for the estimation of the triplet side length. The cylindrical window introduces an offset of the linear calibration that varies non-linearly across the field of view and was compensated for by a function consisting of a 2$^{\mathrm{nd}}$ order polynomial along the streamwise (x) and circumferential (z) axis.

A collimated laser sheet is provided by two high-speed pulsed lasers (2× Innolas Photonics Nanio Air) and introduced to the pipe by a right-angle prism, enabling grazing incidence

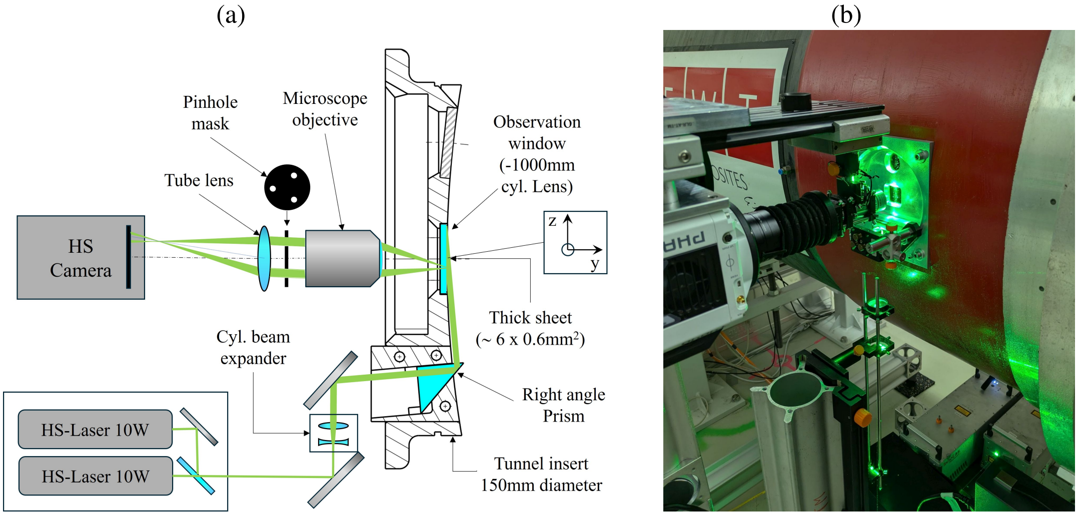

Figure 1. (a) Schematic of the MA-µPTV setup, (b) Photograph of the setup on the test section of the CICLoPE facilty.

Table 1. Acquisition parameters for near-wall turbulent pipe flow MA-µPTV measurements.

Centerline velocity [m/s]	U_{cl}	**5.54**	**7.87**	**10.21**	**14.98**	**20.0**		**30.1**	
Reynolds number	Re_τ	5 940	8 200	10 400	14 900	19 400		28 400	
Friction velocity [m/s]	u_τ	0.201	0.277	0.352	0.502	0.657		0.962	
Viscous length scale [µm]	$l^* = \nu/u_\tau$	78.0	56.4	44.3	31.0	23.7		16.1	
Sampling rate [kHz]	f_{acq}	20	20	20	20	20	40	40	53
Number of sequences		16	16	32	32	32	32	32	32
Samples per sequence	N	14 096	14 096	7 038	7 038	5 550	14 076	14 076	18 736
Independent samples	N_{eff}	140	198	256	376	197	250	377	379
Magnification [µm pixel^{-1}]		1.8	1.8	1.8	1.8	1.8	3.6	3.6	3.6
Image Size [l^*]	$x^+ \times z^+$	47×18	65×25	83×31	119×45	194×58	155×117	228×171	228×128

on the window (see Fig. 1a). Both lasers have an average rated power of 10 W at a pulse repetition rate of 40 kHz and fire simultaneously, providing ≈ 0.5 mJ per pulse. Two cylindrical lenses expand the beam diameter to roughly 6 mm $\times$ 0.6 mm along the streamwise (x) and radial (y) axis.

The flow is seeded with $d_p = [1-2]$ µm long-lasting aerosol droplets from a water-based fog generator (HazeBase Classic, base*M fluid).

Table 1 provides an overview on test points for which sequences were acquired with MA-µPTV. Measurements were performed at centerline velocities of $U_{cl} = 5.2\,\mathrm{m/s}$ up to $30.1\,\mathrm{m/s}$ spanning a shear Reynolds number range of $Re_\tau =$ 5 700 to 28 100. To match the mean flow velocity, the framing rate of the high-speed camera is varied between 20 kHz and 53 kHz with the former resulting in an image size of 2048 pixel $\times$ 768 pixel. At the highest two velocities 2×2 pixel binning was used to achieve the required high sampling rates resulting in images of 1024 pixel $\times$ 768 pixel (Table 1 provides image sizes in viscous units). For each centerline velocity up to 32 sequences consisting of 7 000 to 18 100 images each constitute the basis for the subsequent 3d-PTV. The quantity N_{eff} indicates the number of independent samples based on the eddy turnover time $\tau = R/U_{cl}$.

IMAGE PROCESSING AND 3D-PTV

To minimize the artifacts introduced by window contamination by particle deposition, a sliding minimum over 20 frames is subtracted from each image. Next, particle images are first identified by template matching by convolving the image with a Gaussian template. Then a search is performed on the particle image centroids to find the vertices of triplet candidates. Matching is based on a similarity measure S of the triangle sides $\vec{a}_1$ to a reference vector $\vec{e}_1(x,y,z)$ that is determined by an a priori calibration procedure using a y-traversed mask of pinholes (see Klinner & Willert, 2025 for details).

Once a triplet is identified, the three particle image centers are refined by means of least squares fitting of a 2d Gaussian of predetermined width. The y position is calculated from the mean of y_1, y_2 and y_3. Each value is determined from the length of each triangle side $|\vec{a}_1|$, $|\vec{a}_2|$ and $|\vec{a}_3|$ using calibrated sensitivity. Half of the maximum absolute deviation between the three y-positions serves as measure of reconstruction quality (i.e. disparity δ_y). Fig. 2 shows a sample image at $U_{cl} = 7.7\,\mathrm{m/s}$ with matched triplets for which the maximum accepted disparity is 6 µm.

Using the reconstructed particle positions, Lagrangian particle tracks were initialized with up to four image frames using classical techniques as described by Malik *et al.* (1993) and Ouellette *et al.* (2006). From candidates that are linked in four frames, the track with smallest change in velocity is selected (e.g. minimum acceleration criterion). To continue

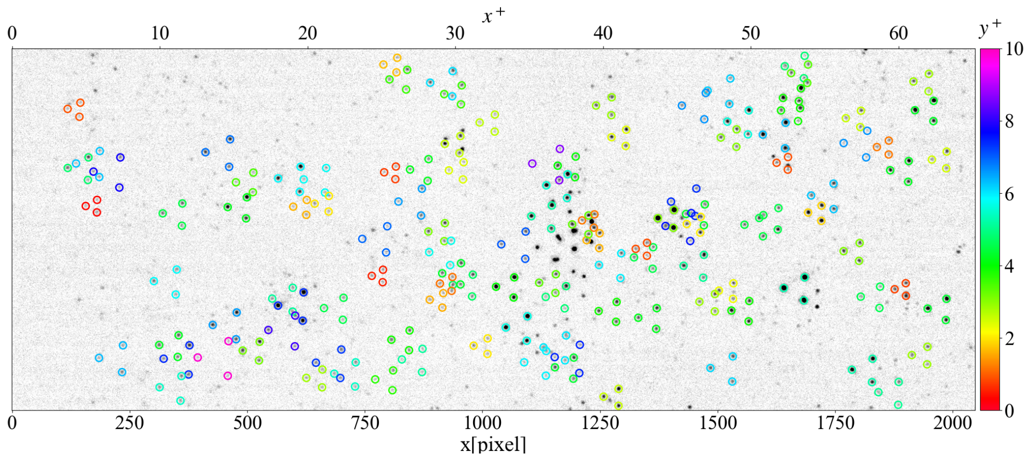

Figure 2. Processed MA-μPTV sample image at $U_{\text{cl}} = 7.7\,\text{m/s}$ ($\text{Re}_\tau = 8\,200$) with detected triplets color-coded by the estimated wall distance.

tracks beyond three members, the predicted displacement toward following frames is based on the velocity difference to the predecessor plus the displacement extrapolated from the acceleration in the previous two frames. For longer tracks, the predictor relies on a cubic polynomial fitted through the last four track members. A new element is assigned if it lies within the relative wall distance change t_y and its distance from the predictor is smaller than a circular search region with radius r_s. Following forward tracking across a sequence of frames, tracks with fewer than a specified number of members t_N are eliminated. With the spurious tracks removed, the entire tracking procedure is repeated for the remaining non-linked particles in backward time association, followed by removal of short tracks. To obtain the particle positions and velocity from the reconstructed track, least-squares regression is applied using a cubic B-spline fitting scheme. Weighting is applied at each vertex, using the disparity of each triplet. To get wall-normal profiles of various statistics (e.g. bin counts, velocities, WSS), a bin-averaging scheme was employed with a bin size of 8 μm, which is smaller than half of the smallest viscous unit. The assignment into equally spaced bins is performed using bilinear weighting.

Fig. 3 shows example profiles of bin densities of tracked particles at $U_{\text{cl}} = 15\,\text{m/s}$ which were used for the optimization of the tracking parameters (e.g. t_y, t_N, r_s). In (a) the enclosing black curve indicates the overall bin density of tracked and untracked particles. The curve is affected by the laser power density, which reaches its maximum at $y = 0.2\,\text{mm}$ and decreases with distance from the wall. For a variation of t_y, Fig. 3 shows that the bin counts and the mean track lengths in the viscous sublayer are largest at $t_y = 0.25$. However, it is assumed that correctly tracked particles maximize the wall gradient. Indeed, the velocity profile in (c) reveals a slight flattening of the wall gradient at $t_y = 0.25$ (wall gradients are provided in the plot legend) while the maximum gradient is achieved at $t_y = 0.1$, which also maximizes the track length within a wall distance range of $0.1\,\text{mm} - 0.2\,\text{mm}$.

To capture additional tracks within the viscous sublayer, the previously described tracking procedure is repeated once on all un-tracked particles using a larger t_y. For $U_{\text{cl}} = 15\,\text{m/s}$, this leads to a further increase in the gradient from $15\,920\,\text{s}^{-1}$ to $16\,000\,\text{s}^{-1}$, corresponding to a friction velocity of 0.497 m/s which underestimates the pressure-based reference by merely 1% (cf. Table 1).

Essential for the estimation of the wall shear stress is a precise knowledge of the wall position. This is achieved using a 2[nd] order polynomial fit of 3d positions of particles stuck to the curved inner surface of the viewing area. As the velocity increased, wall vibrations were observed; these were taken into account in the calculation of the wall shear stress by determining the transient wall position in each individual frame. This offset was then subtracted from the 3d particle positions in each frame prior to particle tracking. At $U_{cl} = 30\,\text{m/s}$ Fig. 4 shows axial vibration amplitudes less then 1 viscous unit at 10.67 Hz, which corresponds to the fan's rotational speed. The WSS relevant wall-normal excursions are limited to $\pm 2\,\mu\text{m}$ ($\approx 0.1\nu/u_\tau$). Based on these data, this MA-μPTV implementation demonstrates a measurement uncertainty of well below 1 μm. An analysis of the probability density function (PDF) of the wall particle positions confirmed a measurement accuracy for individual particles of $\sigma_{x,z} \approx 0.1\,\mu\text{m}$ and $\sigma_y \approx 0.9\,\mu\text{m}$ when low-frequency vibrations are filtered out.

SHEAR STRESS ESTIMATION FROM TRACKS

In general, the viscous skin friction is related to the stream- and spanwise characteristics of the wall shear stress (WSS) vector $\vec{\tau}_w$. This quantity is closely linked to the flow dynamics in the viscous sublayer near the no-slip wall and can be estimated using the tracer particle's velocity $\mathbf{u}$ and its distance from the wall y according to the following relation:

$$\vec{\tau}_w = \mu \left.\frac{\partial \mathbf{u}}{\partial y}\right|_{y=0} = \mu \lim_{y\to 0} \frac{\mathbf{u}(y)}{y} \approx \mu \frac{\mathbf{u}(\Delta y)}{\Delta y} \tag{1}$$

with x, y, z being the streamwise, wall-normal and spanwise coordinates and with μ the dynamic viscosity of the fluid. Since the gradient at the wall cannot be measured directly, the actual WSS can only be approximated using velocity data obtained at finite distance from the wall. In the following, the superscript $(+)$ denotes viscous scaling where the length unit is defined as $l^* = \nu/u_\tau$, with ν being the kinematic viscosity and $u_\tau = \sqrt{\langle\tau_w\rangle/\rho}$ the friction velocity of the boundary layer flow.

The rate of change of the WSS was determined from the particle tracking data during B-spline track fitting, following an approach similar to that described in Willert & Klinner (2025). The particle acceleration vector $\mathbf{a_p} = [a_{p,x}, a_{p,y}, a_{p,z}]$ can be retrieved from particle tracks and is related to the rate

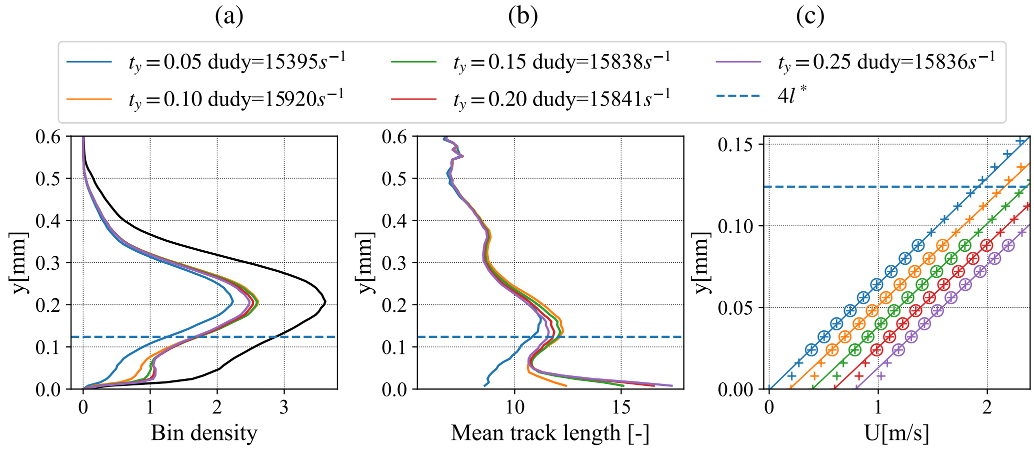

Figure 3. Bin densities (a) and mean track length (b) at $U_{\mathrm{cl}} = 15\,\mathrm{m/s}$ ($\mathrm{Re}_\tau = 14894$) for a variation of t_y (black curve corresponds to the sum of tracked plus un-tracked particles); (c) Near-wall mean velocity profiles (u-offset 0.2 m/s, + measured data, ∘ data included in fit, − linear fit to obtain the wall gradient).

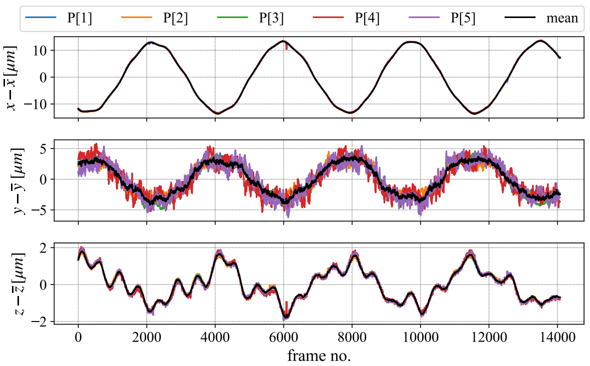

Figure 4. Vibrations of the wall position in an image sequence at U_{cl}=30.1 m/s obtained from five particles fixed to the wall.

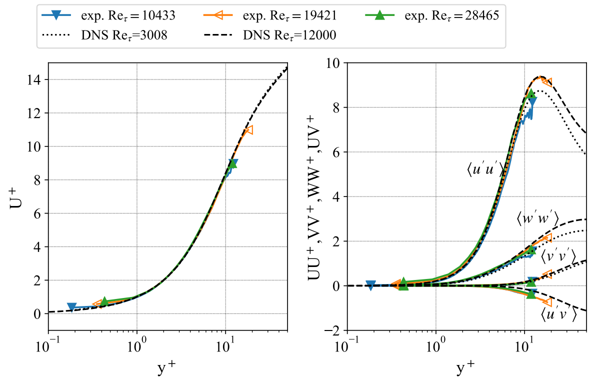

Figure 5. Mean and fluctuating velocities compared to DNS of pipe flow Ahn *et al.* (2015); Pirozzoli (2024)).

of change of the WSS vector:

$$\frac{\partial}{\partial t}(\vec{\tau}_w) = \frac{\partial}{\partial t}\left(\mu \left.\frac{\partial \mathbf{u}}{\partial y}\right|_{y=0}\right) = \mu \left.\frac{\partial \mathbf{a}}{\partial y}\right|_{y=0} \approx \mu\,\frac{\mathbf{a_p}(\Delta y)}{\Delta y}. \quad (2)$$

In the following the symbol $\hat{a}$ refers to this quantity and in effect is the particle acceleration $a_{p,i}$ divided by the wall distance:

$$\hat{a}_i = \frac{\partial \tau_i}{\partial t} = \lim_{y \to 0} \frac{a_{p,i}}{y} \quad (3)$$

PRELIMINARY RESULTS AND OUTLOOK

While the evaluation of the extensive data set is still ongoing, some highlights of the recovered properties of the investigated turbulent pipe flow are presented in the following. The present application of MA-μPTV was primarily aimed to provide time resolved measurements of the unsteady wall shear stress vector $\vec{\tau}_w$ and corresponding streamwise, spanwise and joint probability distributions at friction Reynolds numbers previously unattainable by any other measurement techniques.

Bin-averaged profiles of mean and fluctuating velocities are provided in Fig. 5 and closely match the DNS data up to a wall distance of $y^+ = 5$, accurately reproducing velocities in the viscous layer. As the wall distance increases, faster particle tracks are no longer fully captured, as evidenced by the decrease in bin densities and track length in Fig. 3. This is likely the reason why fluctuations are slightly underestimated at larger wall distances.

Probability density distributions of the two wall shear stress components are presented in Fig. 6 for the complete Reynolds number range investigated herein. It is noteworthy that the distributions exhibit no particular Reynolds number trend – aside from deviations at the tails that can be attributed to the increased influence of measurement noise. This agrees with distributions obtained from DNS of TBL at lower Reynolds numbers Diaz-Daniel *et al.* (2017).

Corresponding joint probability density functions (PDFs) of the WSS components, shown in Fig. 7, exhibit a universality across the investigated Reynolds number range that so far has not been documented experimentally.

Aside from velocity estimates, the reconstructed particle tracks provide estimates of the particle acceleration for which PDFs are compiled in Fig. 8. The distributions are very similar to those of a flat plate TBL at lower Reynolds numbers reported by Willert & Klinner (2025). A slight Reynolds number dependence toward broader distributions can be ascertained. The streamwise acceleration has a slight negative bias that was also observed in near-wall PTV measurements of flat plate

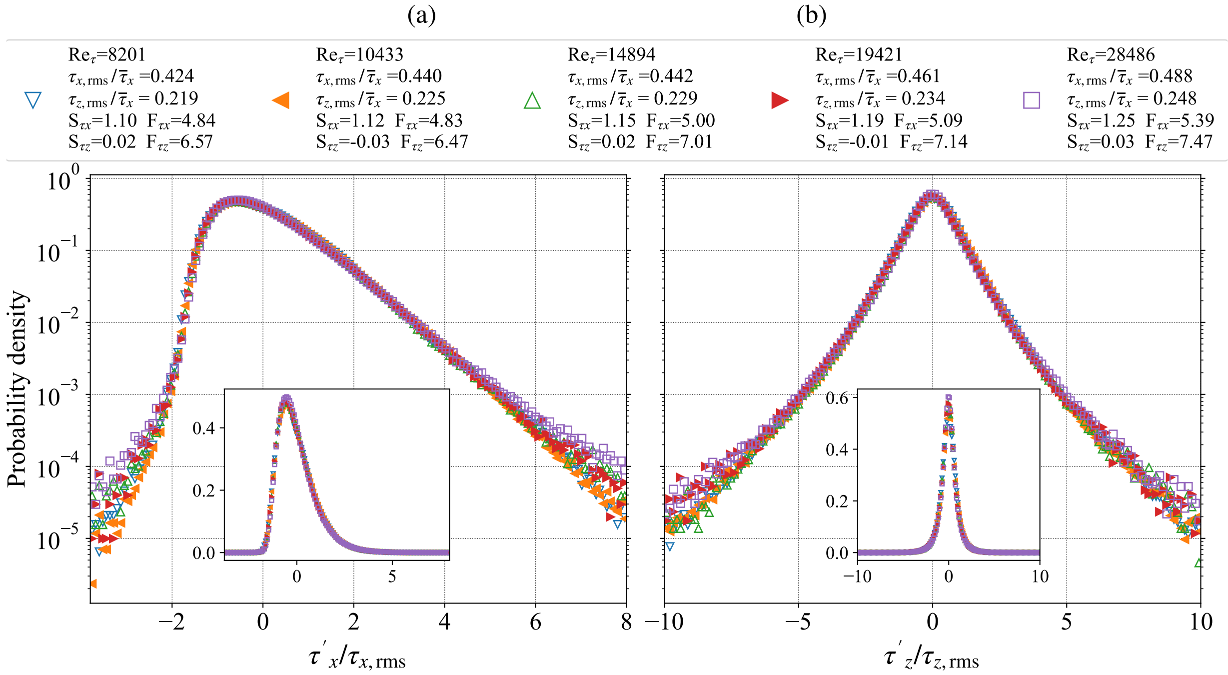

Figure 6. Streamwise (a) and spanwise (b) PDFs of the WSS vector evaluated from particle tracks in the viscous sublayer at $y^+ < 4$.

TBL. Much like the velocity data, the PDF of the accelerations in Fig. 9 also exhibit an essentially Reynolds number independent distribution. The irregularities in the contours, such as bulging, are believed to be artifacts introduced by the complex processing of the acquired image data.

REFERENCES

Ahn, Junsun, Lee, Jae Hwa, Lee, Jin, Kang, Ji-hoon & Sung, Hyung Jin 2015 Direct numerical simulation of a 30R long turbulent pipe flow at *Re* τ = 3008. *Physics of Fluids* **27** (6), 065110.

Diaz-Daniel, Carlos, Laizet, Sylvain & Vassilicos, J. Christos 2017 Wall shear stress fluctuations: Mixed scaling and their effects on velocity fluctuations in a turbulent boundary layer. *Physics of Fluids* **29** (5), 055102.

Klinner, Joachim & Willert, Christian E. 2025 Measurements of the unsteady wall shear stress vector using multi-aperture defocusing microscopic particle tracking velocimetry. *Experimental Thermal and Fluid Science* **163**, 111395.

Malik, N. A., Dracos, Th. & Papantoniou, D. A. 1993 Particle tracking velocimetry in three-dimensional flows **15**, 279–294.

Ouellette, Nicholas T., Xu, Haitao & Bodenschatz, Eberhard 2006 A quantitative study of three-dimensional Lagrangian particle tracking algorithms. *Experiments in Fluids* **40** (2), 301–313.

Pirozzoli, S. 2024 On the streamwise velocity variance in the near-wall region of turbulent flows. *J. Fluid Mech.* **989**, A5.

Talamelli, A., Persiani, F., Fransson, J., Alfredsson, P. H., Johansson, A., Nagib, H., Rüdi, J-D., Sreenivasan, K. & Monkewitz, P. 2009 CICLoPE — a response to the need for high Reynolds number experiments. *Fluid Dynamics Research* **41** (2), 021407.

Willert, C. & Gharib, M. 1992 Three-dimensional particle imaging with a single camera. *Experiments in Fluids* **12** (6), 353–358.

Willert, Christian, Soria, Julio, Stanislas, Michel, Klinner, J., Amili, O., Eisfelder, M., Cuvier, C., Bellani, G., Fiorini, T. & Talamelli, A. 2017 Near-wall statistics of a turbulent pipe flow at shear Reynolds numbers up to 40 000. *J. Fluid Mech.* **826**.

Willert, Christian E. & Klinner, Joachim 2025 Dynamic wall shear stress measurement using event-based 3d particle tracking. *Experiments in Fluids* **66** (2), 32.

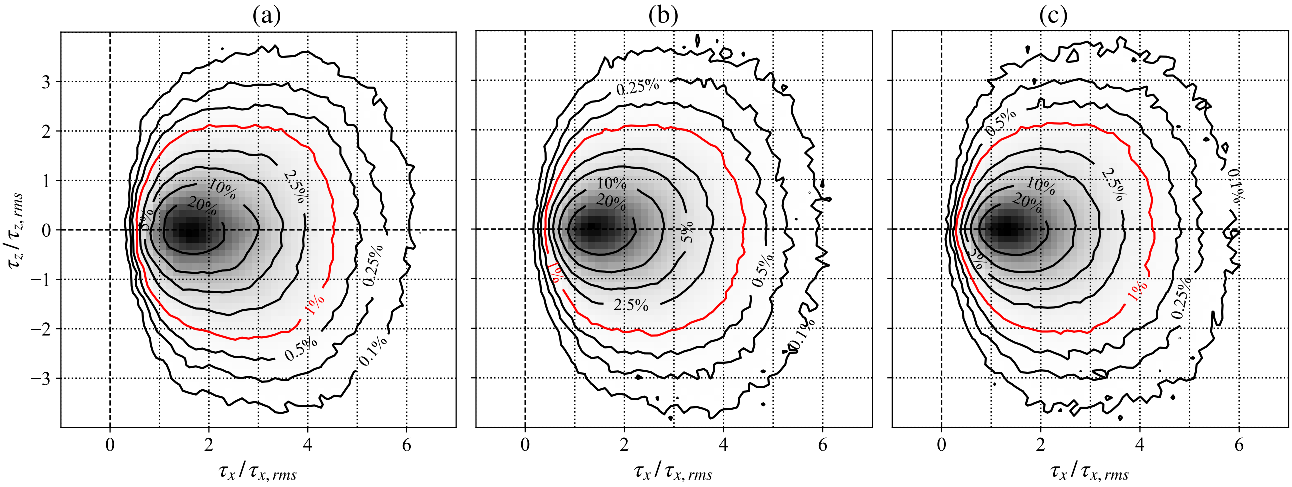

Figure 7. Joint PDF of the WSS vector evaluated from particle tracks in the viscous sublayer at $y^+ < 4$: (a) $\mathrm{Re}_\tau = 10433$ (b) $\mathrm{Re}_\tau = 19421$ (c) $\mathrm{Re}_\tau = 28486$.

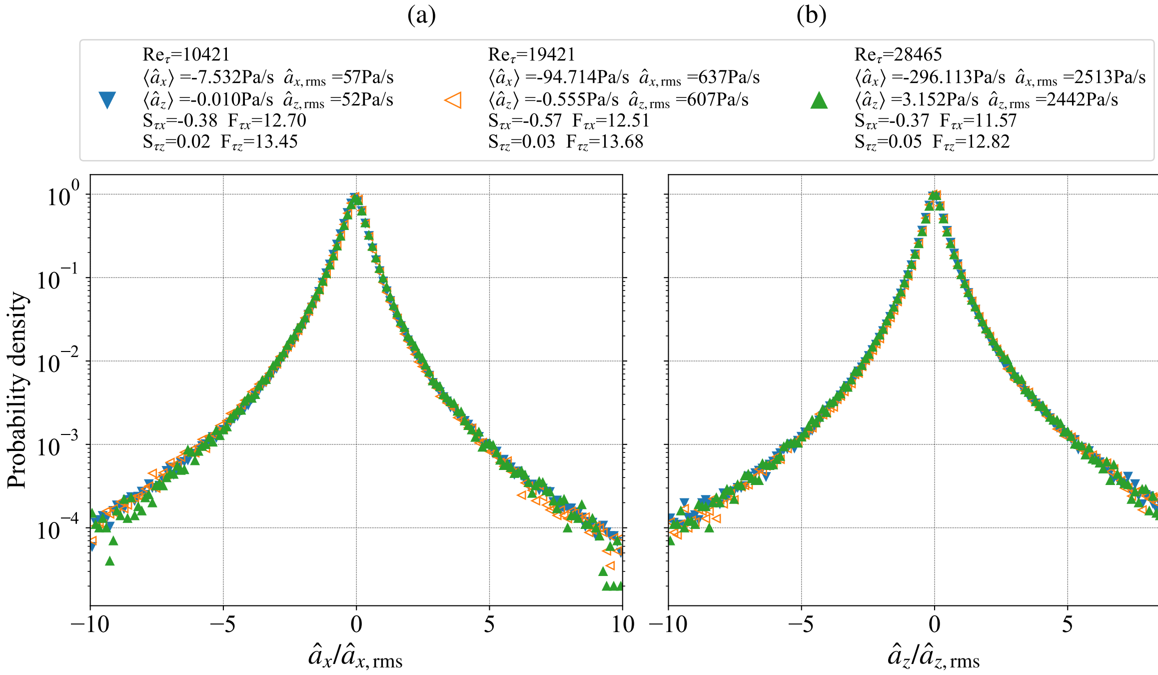

Figure 8. PDFs of WSS accelerations evaluated from particle tracks in the viscous sublayer at $y^+ < 4$: (a) streamwise (b) spanwise component.

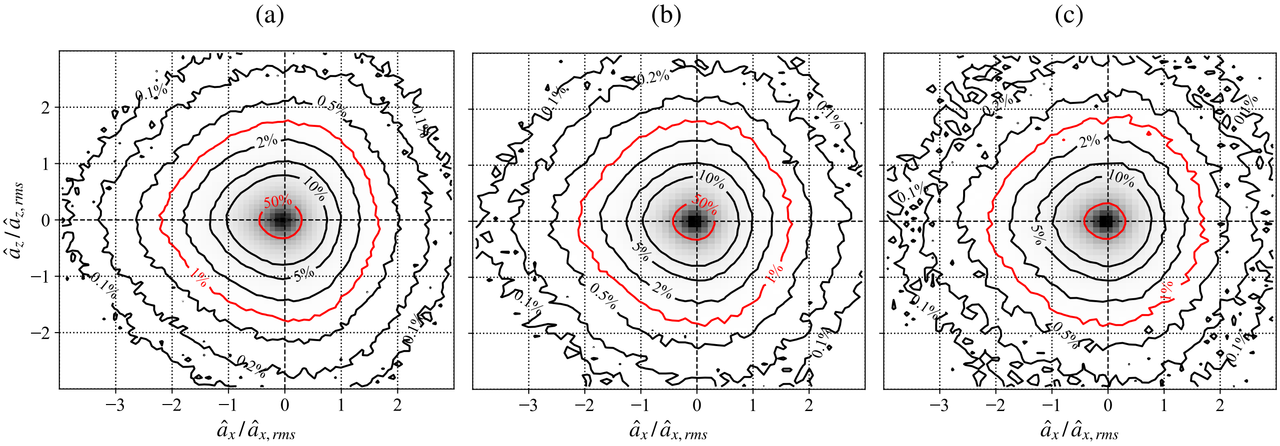

Figure 9. Joint PDF of WSS acceleration evaluated from particle tracks in the viscous sublayer at $y^+ < 4$: (a) $\mathrm{Re}_\tau = 10421$ (b) $\mathrm{Re}_\tau = 19421$ (c) $\mathrm{Re}_\tau = 28465$.